Journal of Sustainable Development of Energy, Water and Environment Systems

http://www.sdewes.org/jsdewes

Year 2026, Volume 14, Issue 1, 1130642

Original Research Article

Production and Physicochemical Characterization of Biodiesel from Croton and Waste Cooking Oil Blends with Carbon-Based Nanoparticles

Abdullahi Aden Hirabe[1]*, Meshack Hawi[2], Mariam Kassim Ali[3], Francis Njoka[4]

[1]Department of Mechanical Engineering, Pan African University Institute for Basic Sciences, Technology and Innovation, Nairobi, Kenya

[2]Department of Mechanical Engineering, Jomo Kenyatta University of Agriculture and Technology, Nairobi, Kenya

[3]Department of Mining, Materials and Petroleum Engineering, Jomo Kenyatta University of Agriculture and Technology, Nairobi, Kenya

[4]Department of Energy, Gas and Petroleum Engineering, Kenyatta University, Nairobi, Kenya

e-mail: aden.abdullahi2023@students.jkuat.ac.ke, mhawi@jkuat.ac.ke, mali@jkuat.ac.ke, njoka.francis@ku.ac.ke

Cite as: Hirabe, A. A., Hawi, M., Ali, M. K., Njoka, F., Production and Physicochemical Characterization of Biodiesel from Croton and Waste Cooking Oil Blends with Carbon-Based Nanoparticles, J.sustain. dev. energy water environ. syst., 14(1), 1130642, 2026, DOI: https://doi.org/10.13044/j.sdewes.d13.0642

ABSTRACT

The search for sustainable alternatives to petroleum diesel has sparked interest in biodiesel production from non-edible feedstocks. This study investigated biodiesel derived from Croton oil and waste cooking oil under optimized transesterification conditions (oil-to-methanol ratios 1:1 and 2:1, 60 C, 400 rpm, 60 min). To further improve the fuel quality, biodiesel was blended with diesel and doped with carbon-based nanoparticles (50 – 100 ppm). Physicochemical characterization of the fuels and nanoparticles was conducted using Fourier Transform Infrared Spectroscopy, Gas Chromatography–Mass Spectrometry, Scanning Electron Microscopy, Transmission Electron Microscopy, and X-ray Diffraction. Conversion efficiencies were reported as 88.13% for Croton oil and 90.96% for waste cooking oil. Viscosity decreased from ~5 mm²/s to ~3.62 mm²/s while the calorific value improved from ~35 MJ/kg to ~40 MJ/kg in pure biodiesel and nanoparticle-doped blends respectively. These improvements demonstrate that nanoparticle-doped biodiesel diesel blends can offer sustainable alternatives to petroleum diesel.

KEYWORDS

Biodiesel, Carbon-based nanoparticles, Doping, Fuel characterization, Transesterification.

INTRODUCTION

The use of petroleum diesel in combustion systems, particularly in on-road engines, has contributed significantly to environmental degradation due to the emission of harmful pollutants. Growing concerns over the depletion of fossil fuel reserves have further intensified efforts to develop alternative, renewable, and cleaner energy sources [1]. Biodiesel has emerged as a promising solution in response to these challenges, offering a renewable substitute for fossil diesel. It is composed of fatty acid methyl or ethyl esters produced through transesterification of vegetable oils, waste cooking oils, or animal fats. With its biodegradability and oxygen-rich composition, biodiesel is regarded as an environmentally friendly fuel [2].

Early biodiesel production largely relied on edible oils such as soybean, rapeseed, and palm [3]. While effective as feedstocks, the large-scale diversion of food crops for fuel has raised concerns about food security, land use change, and environmental sustainability. Expansion of edible oil cultivation can contribute to rising food prices, deforestation, and biodiversity loss, limiting the long-term viability of first-generation biodiesel [4]. These limitations have motivated a shift toward second-generation feedstocks derived from non-edible oils and waste streams. Non-edible oils such as Croton, Jatropha, Karanja, Cottonseed, and microalgae are especially attractive because they avoid food-versus-fuel conflicts, while waste cooking oil (WCO) provides the added advantage of waste valorization and reduced disposal challenges. Together, these feedstocks offer a more sustainable route to biodiesel production.

Despite these advantages, raw bio-oils cannot be used directly in diesel engines because of their high viscosity, low calorific value, and poor oxidative stability [5]. Several methods for converting bio-oils into biodiesel have been developed, including supercritical methanol processing, ultrasonic-assisted transesterification, microemulsion, and conventional transesterification. Among these, transesterification remains the most widely used due to its simplicity, efficiency, and cost-effectiveness [6]. A range of catalysts have been applied, including alkali, acidic, and enzyme-based systems, though enzyme catalysts face limitations due to strict operating requirements. Potassium hydroxide (KOH) and sodium hydroxide (NaOH) are the most common and practical catalysts for transesterification [7].

While biodiesel is suitable for use in compression ignition (CI) engines, its performance is often slightly lower than that of fossil diesel due to higher viscosity and lower energy content. These drawbacks can lead to problems such as poor fuel atomization, incomplete combustion, and carbon build-up when biodiesel is used in high concentrations or directly in diesel engine [8]. To balance these challenges, blends containing up to 20% methyl ester in diesel are generally recommended as substitutes, since higher blends tend to exhibit less favorable engine performance [9].

While the benefits of nanoparticle additives are clear, there is limited research applying carbon-based nanomaterials to second-generation biodiesel feedstocks, particularly non-edible oils like Croton and waste-derived oils such as WCO. This gap is especially relevant in the broader context of sustainable energy systems. For instance, Torres García *et al.* [10] highlighted the importance of friction reduction in Stirling engines for renewable energy viability, while Sulistyo *et al.* [11] addressed the role of green TVET systems in biodiesel-based waste-to-energy education using WCO as a feedstock. Similarly, Leichter *et al.* [12] emphasized the role of biodiesel in life-cycle transitions within urban transport systems, particularly in developing countries, but noted challenges in implementation due to data gaps and policy barriers.

In response to these challenges, researchers have sought strategies to improve the physicochemical and combustion properties of biodiesel to enhance its performance and adoption potential. One of the most promising approaches involves the use of nanoparticle additives (NPs), which have gained traction for their ability to mitigate common biodiesel limitations. These additives improve fuel quality due to their exceptional surface-to-volume ratio and high thermal conductivity, which enhance combustion characteristics and overall engine performance [13]. Among the most promising are carbon-based nanoparticles, such as graphene nanoplatelets (GNPs) and multi-walled carbon nanotubes (MWCNTs), which are environmentally benign and thermally stable. Unlike metal-based nanoparticles, carbon nanomaterials provide stable dispersion, enhance the calorific value of fuels through exothermic reactions, and burn cleanly, leaving no harmful engine deposits. Furthermore, they typically require no surfactants and exhibit minimal agglomeration, ensuring homogeneous mixing in biodiesel-diesel blends [14], [15].

Phan and Tan [16] demonstrated high biodiesel yields (88 – 90%) from waste cooking oil using optimized transesterification parameters. Kafuku and Mbarawa [17] achieved 88%

conversion efficiency for Croton oil, while Kafuku *et al.* [18] attained a 95% yield using a solid super-acid catalyst ($(SO_2)_4)/SnO_2 – SiO_2$), without requiring pre-treatment steps. Several studies have applied nanoparticles to improve biodiesel properties. Gawonou *et al.* [19] showed that doping Croton biodiesel with graphene and graphene oxide (GO) increased calorific value (39.41 to 40.36 MJ/kg) and flash point (40 °C to 64 °C). Kumar *et al.* [20] found that blending graphene (20–60 ppm) with WCOME enhanced density (0.84714 to 0.89124 g/cm³) and energy content, although viscosity increased. Wambui *et al.* [21] observed improvements in calorific value and density when GNPs were added to B20, although viscosity rose from 3.60 mm²/s to 9.757 mm²/s at 100 ppm.

In addition to physicochemical enhancements, carbon nanoparticles also influence engine emissions and performance. Hoseini *et al.* [22] studied the effect of graphene oxide (GO) nanoparticles on a diesel engine fuelled with Oenothera lamarckiana biodiesel (B20) at concentrations of 30, 60, and 90 ppm. GO addition slightly reduced density (0.841 to 0.836 g/cm³), increased heating value (43.87 to 44.37 MJ/kg at 60 ppm), and decreased viscosity (5.721 to 5.554 mm²/s). El-Seesy and Hassan [23] reported that adding 50 ppm of GO, GNPs, or MWCNTs to a JME40B blend slightly increased calorific value up to 37.565 kJ/kg and viscosity increased from 3.34 mm²/s to 3.68 – 3.69 mm²/s with GO and MWCNTs, while GNPs showed a slightly lower value of 3.65 mm²/s.

This study contributes to the field of sustainable biofuels by developing and optimizing biodiesel blends from non-edible Croton oil and waste cooking oil (WCO), addressing both environmental and fuel performance challenges. It explores the use of carbon-based nanoparticles, graphene nanoplatelets (GNPs) and multi-walled carbon nanotubes (MWCNTs), to enhance key fuel properties such as viscosity, calorific value, and flash point. Through comprehensive physicochemical and structural characterization, the research demonstrates that nanoparticle-doped B20 biodiesel blends meet international standards and offer improved combustion potential. This work also provides a low-cost approach to cleaner diesel alternatives and informs future studies on nanotechnology-enhanced biofuels.

These findings underscore the growing interest in nanoparticle-enhanced biodiesel. However, their application in second-generation feedstocks, particularly combinations of Croton oil and WCO, remains underexplored. This study addresses that gap by investigating the production and nanoparticle-enhancement of biodiesel derived from Croton and waste cooking oils. Specifically, it evaluates the effects of GNPs and MWCNTs on key physicochemical fuel properties, aiming to support, low-emission alternatives aligned with global sustainability and circular economy goals.

MATERIALS AND METHODS

This section presents the materials, including the sourced bio-oils, analytical-grade chemicals, and nanomaterials, as well as the methods employed for biodiesel production, preparation of fuel blends, and the analysis of the physicochemical properties of the fuels and their blends.

Materials

Ultra-purified waste cooking oil (WCO) and Croton oil (properties listed in Table 1) were sourced locally. Multi-walled carbon nanotubes (MWCNT) and graphene nanoparticles (GNPs) (properties detailed in Table 2) were purchased from NanoShel Company, India. All other chemicals of analytical reagent grade, such as potassium hydroxide pellets (98.5% purity), methanol (99.9% purity), and phenolphthalein, were commercially obtained from Benchtop Lab Africa and used without further purification.

Table 1. Physical properties of Croton and WCO samples

Property	Units	Croton (Mean ± Std)	WCO (Mean ± Std)
Viscosity at 40 °C	**(**mm^2/s**)**	23.19 ± 1.08	33.60 ± 1.32
Density at 23 °C	(g/cm^3)	0.90 ± 0.01	0.89 ± 0.01
Calorific value	(MJ/kg)	33.09 ± 0.15	32.21 ± 0.14
Acid Value	(mg KOH/g)	4.48 ± 0.05	3.57 ± 0.04
FFA%	(%)	2.26 ± 0.03	1.80 ± 0.03
Iodine number	(g I_2/100 g)	150.58 ± 1.25	136.33 ± 1.18
Moisture Content	(% wt.)	0.07 ± 0.01	0.24 ± 0.02

Table 2 presents the physical characteristics of the MWCNTs and GNPs employed as fuel additives in this study.

Table 2. Graphene Nanoparticles and Multi-Walled Carbon Nanotubes Specifications

Parameter	Multi-walled Carbon Nanotubes	Graphene Nanoplatelets
Company	NANOSHEL	NANOSHEL
Colour	black	black
Morphology	-	Flaky
Diameter/Thickness	10-20 nm	2-4 nm
Length	3-8 µm	~5 µm (± 3%)
Purity	>99%	99.50%
Average interlayer distance	0.34 nm	-
Specific surface area	90-350 m^2/g	-
Bulk density	0.05-0.17 g/cm^3	~ 0.10 g/ml
Real density	1-2 g/cm^3	~ 2.30 g/cm^3

Methods

Biodiesel production. Prior to biodiesel preparation, the acid value of the raw oil was determined to establish whether transesterification or esterification would be used. To determine the acid value, 10 g of oil (croton/WCO) was dissolved in 50 ml of ethanol in a 150 ml beaker and heated to enhance the solubility. A few drops of phenolphthalein indicator were added, and the solution was titrated to the endpoint, which was characterized by the persistent pink colour of the mixture [24]. The low acid value of waste cooking oil (3.57 mg KOH/g) and Croton oil (4.48 mg KOH/g) signified that the transesterification process could be directly used for biodiesel production.

In this process, 200 ml (170.34 g) of refined WCO was poured into the reactor and heated to 60 °C. Then, 1% (w/w) of KOH (relative to the oil mass) was dissolved in 100 ml of methanol (50% v/v relative to the oil). The methanol-KOH mixture was added to the preheated WCO, and the reaction was maintained for 60 minutes under continuous stirring [17]. Croton biodiesel was produced by initially preparing a 1% w/v solution of KOH in methanol, which was then mixed with Croton oil.

The resulted mixture was heated for 60 minutes under continuous stirring at a constant temperature of 60 °C [17], [25]. Upon completion, all reaction products were transferred to a separation funnel and left overnight to allow the phase separation of biodiesel and glycerine. The biodiesel, containing impurities such as glycerine, methanol, and KOH catalyst, was then washed several times with warm distilled water at 50 °C to remove impurities. The remaining methanol and water in the biodiesel were removed by heating the product to 110 °C and holding it at this temperature until all water bubbles vanished. Eq. (1) was used to determine the biodiesel yield under varying transesterification conditions, while **Figure 1** summarizes the process of biodiesel production [16], [17], [19]:

$$Yield\ (\%) = \frac{Mass\ of\ pure\ Biodiesel}{Mass\ of\ the\ Crude\ Oil} \tag{1}$$

The equation suggests that yield is highly sensitive to oil-methanol ratio, which influences transesterification kinetics, methanol-oil miscibility, and catalyst activity. Using this equation allows quantitative comparison of biodiesel output at different oil-methanol ratio, ensuring selection of the optimal operating condition.

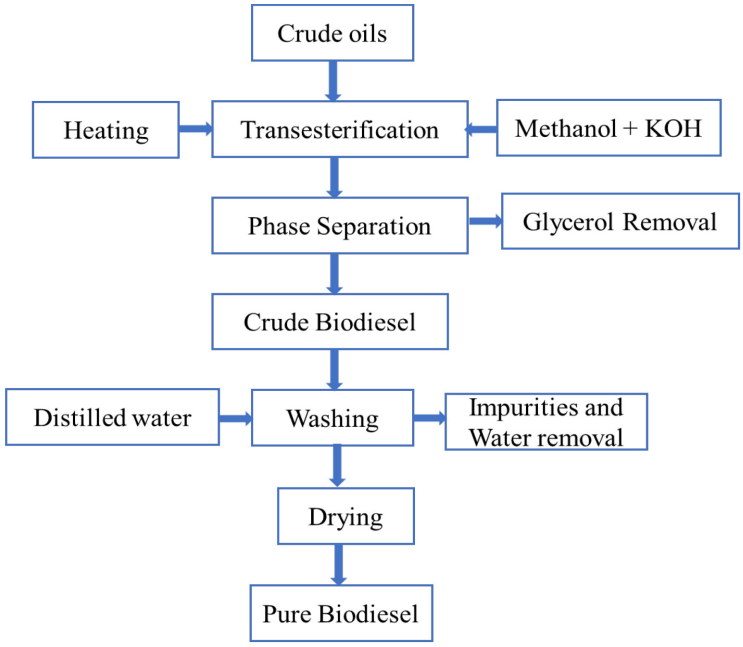

Figure 1. Schematic diagram of the transesterification process for biodiesel production

Preparation of fuel blends. To investigate blending effects, various fuel mixtures of petroleum diesel, WCO and Croton biodiesel, and nanoparticle blends outlined in **Table 3** were studied. Different WCO and Croton biodiesel ratios were tested to find the optimal ratio for favourable properties, as shown in the supplementary information. To form WCB, an 80% WCO biodiesel and 20% Croton biodiesel blend was used. To produce B20, 20% WCB was mixed with 80% petroleum diesel and stirred at 1500 rpm for 20 minutes.

To study the effect of nanoparticles, 1 litter of B20 blend was mixed with different nanoparticle concentrations (50 ppm, 75 ppm, and 100 ppm) based on related previous studies [26]. The required nanoparticle (GNPs and MWCNTs) mass was accurately weighed using a high-precision ENTRIS224-1S analytical balance with an accuracy of 0.0001 g. To ensure uniform dispersion of nanoparticles in the fuel, the mixture was subjected to ultrasonication for 20 minutes at a frequency of 24 kHz using a Hielscher ultrasonicator (Model CL-188).

Table 3. Biodiesel blends description

Fuel sample	Description
D100	100% diesel
W100	100 % Waste cooking oil biodiesel
C100	100 % Croton oil biodiesel
B100	100% WCB (80% Waste Cooking and 20 % Croton Biodiesel)
B20	20% WCB + 80% diesel
B20+G50 ppm	20% WCB + 80% diesel + 50 ppm of graphene
B20+G75 ppm	20% WCB + 80% diesel + 75 ppm of graphene
B20 + G100 ppm	20% WCB + 80% diesel + 100 ppm of graphene
B20+MWC50 ppm	20% WCB + 80% diesel + 50 ppm of MWCNTs
B20+MWC75 ppm	20% WCB + 80% diesel + 75 ppm of MWCNTs
B20+MWC100 ppm	20% WCB + 80% diesel + 100 ppm of MWCNTs

Physicochemical characterizations of fuels and nanoparticles. Gas Chromatography-Mass Spectrometry was performed with GCMS (Model-QP-2010 SE) to analyse the chemical composition of Croton oil and waste cooking oil (WCO). FTIR, was identified as functional groups of raw Croton oil, WCO, and biodiesel products, including 100% Croton (C100) and waste cooking biodiesel (W100), with/without nanoparticles and petroleum diesel [27].

The physicochemical properties of D100, B100, and B20, as well as B20 blends doped with graphene and multi-walled carbon nanotubes (MWCNTs) at concentrations of 50, 75, and 100 ppm, were evaluated. Density, viscosity using a Viscometer, Model AN-823 m, calorific value with a Bomb Calorimeter, Model C200/3/1, flash point using a Pensky Martens apparatus, Model K16270, water content, iodine number, and cold filter plugging point were also conducted. The measured properties were then compared with the standard specifications of EN 14214 and ASTM D6751 to determine the effects of nanoparticle additives on the fuel blends.

The morphology of carbon-based nanoparticles (CBNPs) was examined using scanning electron microscope, and transmission electron microscope, SEM (JEOL, JSM-6010 LV) and TEM (JEOL JEM-2100 F), while their structural analysis was performed using X-ray diffraction, XRD (Shimadzu XRD-6100). The average particle sizes of the graphene nanoparticles and MWCNTs were evaluated using the Scherrer equation as illustrated in eq. (2) [28], [29]:

$$Particle\ Size\ (\text{nm}) = \frac{0.9 \times 0.154}{\beta \sin\theta}(\text{nm}) \quad (2)$$

It indicates the effective surface area of nanoparticles, which dictates their thermal conductivity and catalytic enhancement of combustion, depends on crystallite size. Since biodiesel combustion and viscosity are temperature-dependent, this equation indirectly links nanoparticle structural stability to their performance in biodiesel blends under varying thermal conditions.

RESULTS AND DISCUSSION

This section presents the results and discussion on biodiesel production, the chemical composition of the fuel samples, the characterization of the nanoparticles, and the physicochemical properties of the prepared biodiesel and its blends.

Biodiesel Production

Several samples were prepared to identify the optimal reactant ratio that produces an acceptable and economically feasible yield. **Figure 2** illustrates the Separation Phase, Washing Process and Pure Biodiesel from the transesterification process, while **Table 4** presents the corresponding yields from each sample of the oil-to-methanol ratios.

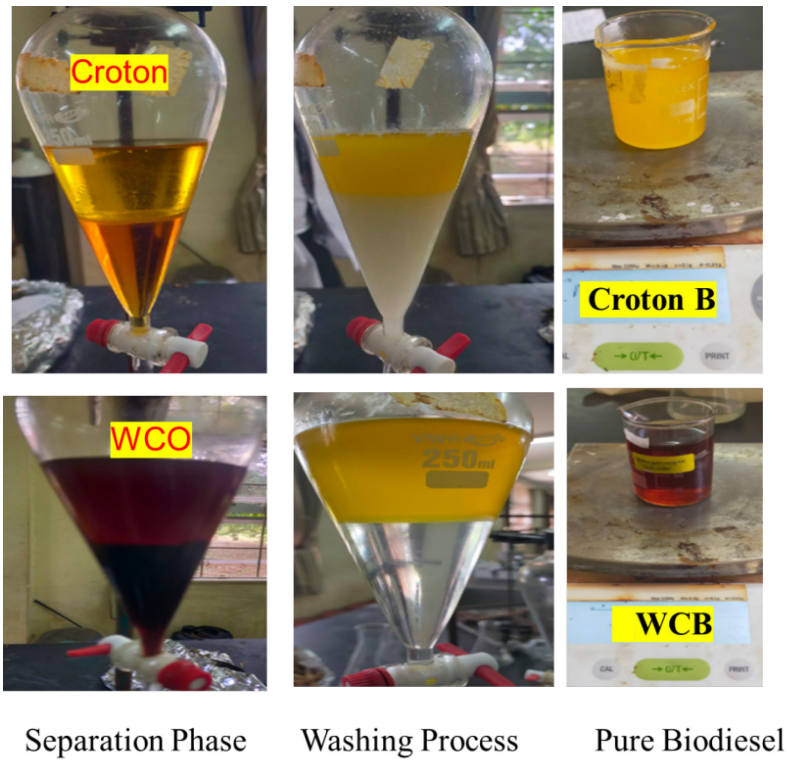

Figure 2. Separation phase, washing process and pure biodiesel

Table 4. Test Samples and Conversion Rates of Biodiesel Yields

Property	Croton oil			WCO		
	Sample 1	Sample 2	Sample 3	Sample 1	Sample 2	Sample 3
Crude oils (ml)	100	200	200	200	200	200
Methanol (ml)	100	400	100	200	400	100
Oil to methanol volume ratios	1:1	1:2	2:1	1:1	1:2	2:1
Potassium hydroxide (KOH) (g)	1	1	1	1	1	1
Mass of crude oils	85.15	170.34	169.89	170.34	170.25	170.11
Mass of pure biodiesel	75.05	152.85	137.09	153.95	157.84	154.74
Yield (%)	88.13	89.73	80.69	90.37	92.71	90.96

Based on the experimental results and overall conversion efficiency, Sample 2 exhibits the highest biodiesel yield for both Croton oil (89.73%) and WCO (92.71%). However, other critical parameters influenced the final sample selection. For Croton oil, Sample 1, with an oil-to-methanol ratio of 1:1, was chosen as the most suitable option due to its high yield of 88.13%, which is close to the maximum yield. This selection is based on its comparable yield of 88.13%, which aligns with the findings reported by [17], [19]. For WCO, Sample 3 (2:1 oil-to-methanol ratio) was found to be the most cost-effective option, achieving a yield of 90.96%, which is very close to that of Sample 2, while using less methanol. This yield also aligns with the 90% reported by Phan and Tan [16].

Although Sample 2 achieved the highest biodiesel yield for both Croton oil and WCO, its high methanol consumption makes it less cost-effective for large-scale applications. However, Sample 1 (Croton oil) and Sample 3 (WCO) offered slightly lower yields but provided a better balance between yield, methanol efficiency, and economic viability, making them more sustainable and practical options for real-world biodiesel production.

Characterization of the Nanoparticles

X-ray Diffraction Analysis. The phase composition and crystal structure of the nanoparticle are examined using X-ray diffraction as described in Figure 3. Figure 3A and Figure 3B depict the XRD pattern of the graphene nanoparticles and MWCNTs, respectively.

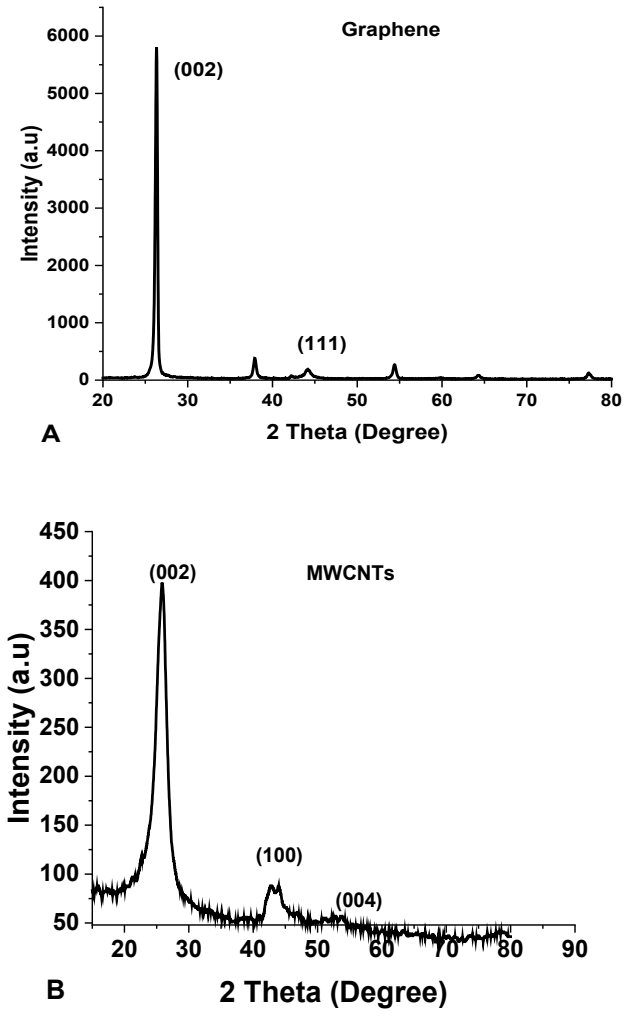

Figure 3. The XRD pattern of the graphene nanoparticles (A), and MWCNTs (B)

The formation of -OH and -COOH groups is responsible for the intense peak (2 theta) at around 25.7° – 26.3° indexed to (002) hkl values in both XRD spectra, confirming the highly graphitic structure of the Graphene and MWCNT particles [12]. Graphene sheets are stacked in a concentric cylindrical shape, and the nanotubes are multi-walled. The peak at 44.3° – 46.3° in both spectra, which corresponds to (100) hkl values, is associated with JCPDS fl.no: 41 – 1487, which validates the preservation of graphite structure following the reduction procedure process [27]. The average particle sizes of the Graphene nanoparticles and MWCNTs determined by the Scherrer equation were 24.2 nm and 1.5 nm, respectively.

Transmission Electron Microscopy Analysis. **Figure 4** shows the TEM images of graphene nanoparticles and MWCNTs. The GNPs are spherical and sheet-like (**Figure 4A**) while MWCNTs are tubular in shape (**Figure 4B**).

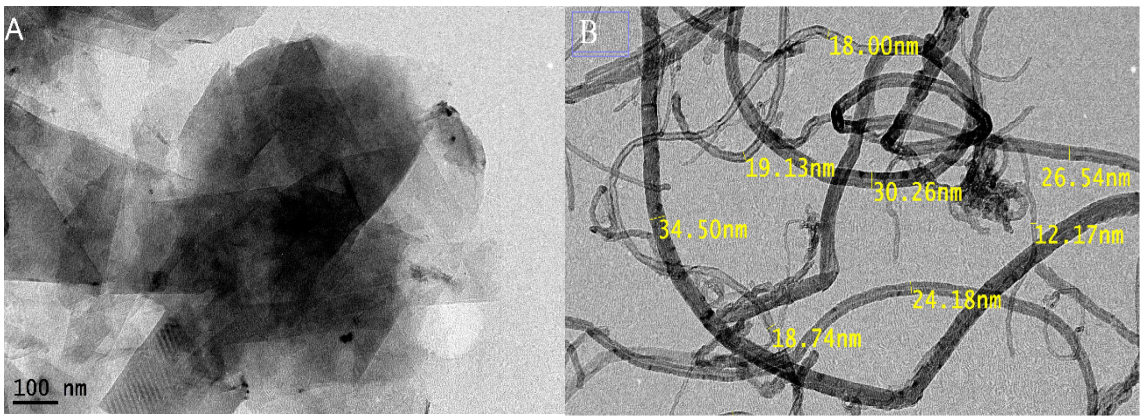

Figure 4. TEM images of Graphene nanoparticles (A), and MWCNTs (B)

The special qualities and benefits: of graphene nanoparticles include exceptional mechanical and electrical characteristics, exceptional charge carrier mobility, high thermal conductivity, high surface area, and exceptional mechanical strength [28]. The properties of high thermal conductivity and high surface area have been reported to enhance the fuel quality and improve engine combustion characteristics [29]. Using high-magnification TEM, the outer diameters of MWCNTs were measured using the point-to-point inbuilt measuring tool and found to be in the range of 12mm to 35 nm.

Scanning Electron Microscopy Analysis. **Figure 5** shows the surficial characteristics of the nanoparticles. **Figure 5A** shows the SEM images of graphene nanoparticles, while **Figure 5B** shows the SEM images of the MWCNTs.

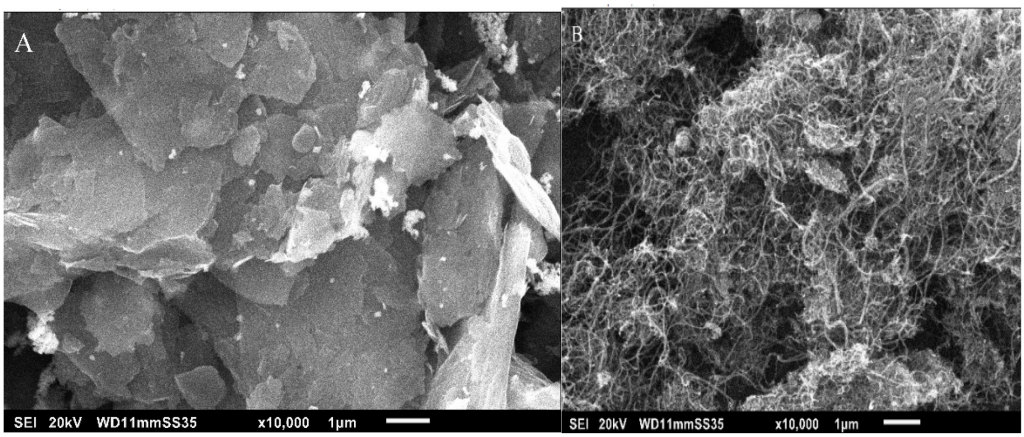

Figure 5. SEM images of G (A), and MWCNTs (B)

The numerous lamellar layer structures of Graphene nanoparticles are visible, and the SEM images clearly show the margins of separate sheets as shown in **Figure 5A**. The asymmetric images show confined spaces stacked on top of one another. Additionally, it is observed that the GNP sheets have thicker edges, which could be attributed to the oxygen-containing functional groups that are joined at the margins of graphene nanoparticles **[30]**. The MWCNTs are tubular in shape and are arranged in bundles with smooth surfaces (**Figure 5B**) **[31].**

Chemical Composition Analysis of the Fuels

Gas Chromatography-Mass Spectrometry. The chemical compositions of fatty acid methyl esters (FAMEs) derived from WCO and Croton oil are presented in **Table 5**. The results reveal clear differences in their saturation levels, which strongly influence fuel properties and stability. WCO FAME is dominated by monounsaturated fatty acids, with oleic acid methyl ester (C18:1) as the major component (66.8%), followed by palmitic acid methyl ester (C16:0, 22%) and stearic acid methyl ester (C18:0, 9.1%). These saturated and monounsaturated fractions account for more than 97% of the composition. The relatively high proportion of oleic acid provides WCO FAME with enhanced oxidative stability and resistance to rancidification, while the presence of saturated C16:0 and C18:0 esters contribute to a higher cetane number and improved combustion stability, albeit at the cost of poorer cold flow behaviour due to crystallization at low temperatures. Croton oil FAME exhibits a markedly different profile, being highly unsaturated, with linoleic acid methyl ester (C18:2) as the predominant component (70%), along with notable fractions of oleic acid (C18:1, 9.2%) and stearic acid (C18:0, 10%). The high degree of polyunsaturate enhances cold flow properties but makes Croton biodiesel more prone to oxidative degradation, reducing storage stability and increasing susceptibility to rancidification. Interestingly, Croton oil also contains small amounts of non-standard fatty acids such as C19:0 (2.80%) and long-chain unsaturated C20:1 (1.9%), which may influence fuel lubricity and thermal behaviour.

These compositional differences indicate that WCO FAME, with its higher oleic acid content, offers better oxidative stability and combustion efficiency, while Croton oil FAME, due to its high linoleic acid proportion, contributes superior cold flow performance but at the expense of storage stability. Thus, blending the two feedstocks balances these complementary properties, improving overall biodiesel quality by combining the oxidative stability of WCO with the cold flow benefits of Croton oil.

Table 5. Chemical composition of Croton and Waste cooking oils

Fatty Acid	Total fatty acid methyl ester (wt.%)	
	WCO	Croton oil
C14:0	0.1	0.1
C16:0	22	6.6
C18:0	9.1	10
C18:1	66.8	9.2
C18:2	0.2	70
C19:0	-	2.8
C20:0	0.4	0.4
C20:1(cis)	0.7	1.9

Fourier Transform Infrared Spectroscopy Analysis. FTIR analysis was conducted on Croton oil, WCO, C100, W100, B20, and B20 blends with varying concentrations of

nanoparticles (50 ppm, 75 ppm, and 100 ppm) in the 400 – 4000 cm^{-1} range as shown in **Figure 6**. FTIR analysis, as shown in **Figure 6A**, presents the spectra of diesel, WCO, C100, W100, and B20 to identify functional groups of the fuels. A distinct peak at ~3741 cm^{-1} was observed in diesel, C100, WCO, W100, and B20, which corresponds to O–H stretching vibrations (COOH groups), while Croton oil lacked this peak, showing no evidence of hydrogen bond formation [32]. All fuels displayed strong peaks at 2929 and 2858 cm^{-1}, indicating the presence of C–H asymmetric stretching vibrations of CH_2 and CH_3 groups, characteristic of the alkane family [19]. Additional peaks were observed at 1745 cm^{-1} (C=O in esters [33]), between 1451 – 1460 cm^{-1} (CH_2 bending [34]), and at 1165 –1175 cm^{-1} (C–O vibrations [35]). WCO and C100 also showed a prominent peak at 720 cm^{-1}, related to C–H out-of-plane deformation and C-S stretch [36].

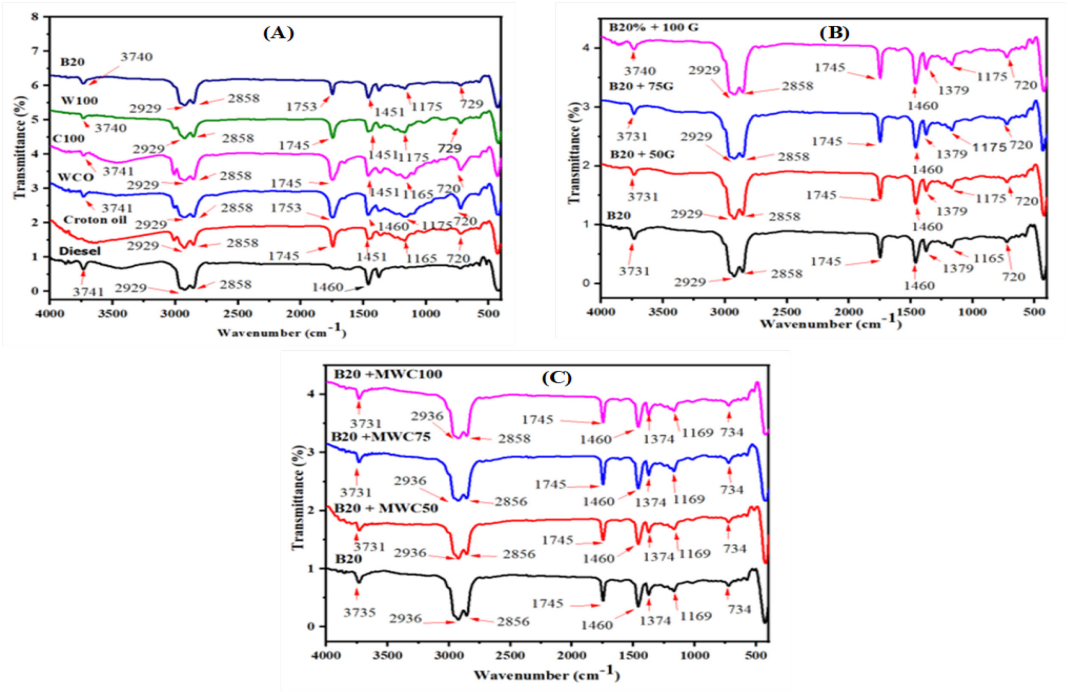

Figure 6. FTIR spectra of diesel, Croton oil, WCO, C100, W100, B20 (A), B20 with GNPs (B), and B20 with MWCNTs (C)

Figure 6B and **Figure 6C** represent the FTIR spectra of biodiesel blends with varying concentrations of nanoparticles. The addition of graphene and MWCNTs at different levels (50 ppm, 75 ppm, and 100 ppm) influenced the composition of the B20 blend, as evidenced by variations in peak intensities. Notably, peaks appearing between 3731 cm^{-1} and 3740 cm^{-1} for B20, graphene, and MWCNT-doped biodiesel blends are more appropriately assigned to O–H stretching vibrations of COOH groups, rather than to C–H asymmetrical stretching. Significant peaks were also observed between 2856 cm^{-1} and 2936 cm^{-1}, corresponding to the C–H stretching vibrations of methylene (CH_2) and methyl (CH_3) groups, which are typical of alkanes [16]. This observation aligns with previous results reported by Gawonou *et al.* [19] and Nespeca *et al.* [36].

Additionally, a strong peak was recorded at 1745 cm^{-1}, characteristic of C=O stretching in ester groups [37]. Nandiyanto *et al.* [38] reported that peaks in the 1800 – 1700 cm^{-1} range correspond to ester carbonyl vibrations, consistent with our findings and those of Wambui *et al.* [21]. Slightly pronounced peaks were also observed between 1374 cm^{-1} and 1460 cm^{-1}, attributable to C–H bending vibrations of CH_2 in alkanes [39]. Weak peaks around 1165 cm^{-1} represent C–O stretching in esters, which El-seesy *et al.* [40] indicated occur between 1125 – 1195 cm^{-1}. Furthermore, C–H out-of-plane bending vibrations were observed in all fuels between 720 – 734 cm^{-1} [21].

The incorporation of graphene and MWCNTs caused subtle shifts in peak positions. For B20 blends with graphene, signal intensities increased with higher nanoparticle concentrations (50–100 ppm). Similar results were observed in MWCNT-doped fuels, where the peak wavenumbers were slightly higher than in graphene-doped blends. Additionally, MWCNT-doped fuels showed progressively increased peak intensity with higher doping levels. These shifts and changes in peak characteristics highlight interactions between nanoparticles and biodiesel, suggesting possible catalytic or surface-mediated mechanisms. This supports the role of carbon-based nanoparticles in improving the composition and functional group characteristics of biodiesel – diesel blends.

Fuel Physicochemical Properties

Table 6 presents the measured physicochemical properties of the fuel samples, highlighting the comparative effects of graphene nanoplatelets (GNPs) and multi-walled carbon nanotubes (MWCNTs) at varying concentrations on fuel characteristics.

Table 6. Physicochemical Properties of diesel, biodiesel, and their blends with Graphene and MWCNT Nanoparticles

Fuel Sample	Viscosity at 40 °C (mm^2/s)	Density at 15 °C (g/cm^3)	Calorific Value (MJ/kg)	Flash Point (°C)	CFPP (°C)	Water Content (% wt.)	Iodine Number (g I_2/100 g)
Diesel	2.99 ± 0.05	0.840 ± 0.002	42.40 ± 0.15	45 ± 1	–15 ± 1	0.02 ± 0.01	6 ± 1
C100	5.96 ± 0.08	0.860 ± 0.002	35.32 ± 0.20	80 ± 2	–3 ± 1	0.06 ± 0.01	92 ± 3
W100	5.42 ± 0.07	0.861 ± 0.003	36.05 ± 0.18	70 ± 2	+2 ± 1	0.07 ± 0.01	78 ± 2
B20	3.77 ± 0.06	0.852 ± 0.002	39.41 ± 0.15	40 ± 1	–10 ± 1	0.04 ± 0.01	35 ± 2
B20 + G50 ppm	3.79 ± 0.06	0.854 ± 0.002	39.42 ± 0.16	35 ± 1	–10 ± 1	0.04 ± 0.01	36 ± 2
B20 + G75 ppm	3.76 ± 0.05	0.857 ± 0.002	39.60 ± 0.14	65 ± 2	–11 ± 1	0.04 ± 0.01	37 ± 2
B20 + G100 ppm	3.85 ± 0.07	0.857 ± 0.002	40.10 ± 0.17	45 ± 2	–11 ± 1	0.05 ± 0.01	38 ± 2
B20 + MWC50 ppm	3.92 ± 0.08	0.858 ± 0.002	39.57 ± 0.15	75 ± 2	–11 ± 1	0.05 ± 0.01	36 ± 2
B20 + MWC75 ppm	3.94 ± 0.08	0.859 ± 0.002	40.20 ± 0.18	90 ± 2	–12 ± 1	0.05 ± 0.01	37 ± 2
B20 + MWC100 ppm	3.62 ± 0.07	0.860 ± 0.002	40.52 ± 0.20	65 ± 2	–12 ± 1	0.06 ± 0.01	38 ± 2
EN 14214	3.5 – 5.0	0.86 – 0.90	35 – 40	≥120	–	≤0.05	≤120
ASTM D6751	1.9 – 6.0	–	37 – 40	≥93	–	≤0.05	–

Cold Filter Plugging Point, Water Content and Iodine Number. The cold filter plugging point (CFPP) of diesel, biodiesel, and their blends is presented in **Table 6** as a critical indicator of cold flow properties. Pure diesel exhibited the most favourable CFPP of –15 °C, highlighting its excellent operability under low-temperature conditions. In contrast, Croton biodiesel (C100) and WCO biodiesel (W100) showed poorer cold flow performance, with CFPP values of –3 °C and +2 °C, respectively. The higher CFPP of W100 is attributed to its larger proportion of saturated fatty acids, which tend to crystallize at low temperatures, thereby increasing the likelihood of fuel filter blockage. These results confirm that biodiesel generally suffers from inferior cold flow behaviour compared to diesel, posing potential challenges for reliable operation in cold climates.

The blended biodiesel (B20) significantly improved cold flow characteristics, with a CFPP of –10 °C, due to dilution with diesel. Incorporation of graphene and MWCNT nanoparticles further enhanced these properties. B20 doped with GNPs at 75 – 100 ppm reduced CFPP to –11 °C, while MWCNT-doped blends achieved even better cold flow, reaching – 12 °C at 75 and 100 ppm. This trend suggests that nanoparticles may interfere with crystal formation by promoting uniform dispersion and altering intermolecular packing within the fuel matrix. Improved cold flow properties are practically important, as they reduce the risk of fuel line blockages and filter plugging in cold conditions, ensuring reliable ignition and stable combustion during winter operation.

Water content values across all biodiesels and blends were below the EN 14214 limit of 0.05%, indicating effective purification and minimizing risks of microbial growth, phase separation, and corrosion in storage tanks and fuel lines. Similarly, iodine numbers reflected the degree of unsaturation: Croton biodiesel (92 g I_2/100 g) was highly unsaturated and more prone to oxidation, while WCO biodiesel (78 g I_2/100 g) exhibited comparatively better oxidative stability. Blends (B20 and nanoparticle-doped variants) showed much lower iodine numbers (35 – 38 g I_2/100 g), indicating reduced susceptibility to oxidative degradation and extended storage stability. The results indicate that nanoparticle doping not only enhances energy content but also improves low-temperature operability, oxidation resistance, and safety margins. This makes Croton – WCO biodiesel blends viable alternatives that comply with major biodiesel standards while minimizing operational risks in diesel engines, improving efficiency, and reducing pollutant formation.

Density and viscosity. **Figure 7** presents the evaluated density and viscosity of the different fuel samples to evaluate the effect of blending biodiesel with nanoparticles. **Figure 7A** presents a pure diesel (D100) had the lowest density, while pure biodiesel samples of Croton biodiesel (C100) and waste cooking biodiesel (W100), and the biodiesel blend (B20) showed higher densities. This rise could be attributed to the higher molecular weight and more complex chemical makeup of biodiesel, as noted by Keera *et al.* **[41]**. Adding graphene nanoplatelets (GNPs) to B20 blends increased the density, in the range of 0.85413 g/cm³ to 0.85731 g/cm³ at concentrations of 50 ppm, 75 ppm, and 100 ppm. These densities exceeded those of both B20 and diesel fuels, showing a clear trend where higher GNP concentrations result in slightly higher fuel density **[42]**. On the other hand, the B20 blends containing multi-walled carbon nanotubes (MWCNTs) exhibited slightly higher and more consistent density values, ranging from 0.85717 g/cm³ to 0.85979 g/cm³ at concentrations of 50 ppm, 75 ppm, and 100 ppm. These densities were marginally higher than those of the graphene-enhanced blends.

A similar pattern of marginal increase in fuel density was reported by Wambui *et al.* **[21]**, who studied Croton-oleander biodiesel blended with diesel (OCB20) enhanced with GNPs with the same concentration, recording densities of 0.850 g/cm³, 0.852 g/cm³, 0.854 g/cm³, and 0.856 g/cm³, for OCB20, OCB20+50G, OCB20+75G, and OCB20+100G, respectively. Similarly, Debbarma *et al.* **[26]** observed that a diesel and palm biodiesel blend (B30) doped with GNPs exhibited densities of 0.848 g/cm³, 0.849 g/cm³, and 0.850 g/cm³ at the same concentrations. A comparable trend was also reported by Sadhik and Anand **[43]**, who investigated carbon

nanotube-enhanced Jatropha Methyl Ester blends at concentrations of 25 ppm, 50 ppm, and 100 ppm, reporting densities of 0.8972 g/cm³, 0.8978 g/cm³, and 0.8994 g/cm³, respectively. A consistent rise in fuel blend density with increasing nanoparticle concentration has been observed for graphene and multi-walled carbon nanoparticles. The GNPs increase density due to their high specific surface area, mass, and planar structure, which promotes uniform dispersion and molecular packing [44]. The MWCNTs exhibit a slightly greater and more stable increase due to their tubular shape and high aspect ratio, which allow for stronger molecular interactions, the formation of an entangled network within the fuel matrix, and reduced intermolecular gaps [45]. In practice, higher densities can influence injection timing and spray penetration in diesel engines, potentially altering combustion phasing and pollutant formation.

Viscosity analysis as illustrated in the **Figure 7B** revealed a consistent trend where pure diesel exhibited the lowest viscosity at 2.99 mm²/s, followed by B20 at 3.77 mm²/s. However, C100 and W100 showed higher viscosities of 5.96 mm²/s and 5.42 mm²/s, respectively, reflecting the typical higher molecular weight and polarity of biodiesel components than petroleum diesel. The introduction of nanoparticles into B20 further influenced the viscosity of the blends. Specifically, B20 blended with graphene nanoplatelets recorded viscosities of 3.79 mm²/s (G50), 3.76 mm²/s (G75), and 3.85 mm²/s (G100), while B20 blended with multi-walled carbon nanotubes exhibited values of 3.92 mm²/s (MWC50), 3.94 mm²/s (MWC75), and 3.62 mm²/s (MWC100). El-Seesy [46], conducted a comprehensive study that investigated carbon nanotube-enhanced Jatropha Methyl Ester blends at concentrations of 10 mg/l, 20 mg/l, 30 mg/l, 40 mg/l, and 50 mg/l of MWCNTs, reporting viscosities of 4.1 mm²/s, 4.19 mm²/s, 4.25 mm²/s, 4.31 mm²/s, and 4.35 mm²/s, respectively. The rise in viscosity with increasing nanoparticle concentration results from agglomeration and microstructure formation, all of which restrict fluid flow. MWCNTs, due to their tubular and entangled structure, slightly increase viscosity more than graphene nanoplatelets, which have a flat, layered form that allows better dispersion and lower resistance [47].

Viscosity is one of the most critical parameters for fuel performance, as higher viscosity can delay injection, reduce atomization quality, and increase the risk of incomplete combustion, leading to carbon deposits, injector coking, and higher emissions of particulates and CO. Despite the marginal increases observed, all viscosities in this study remained within ASTM D6751 and EN 14214 standards, confirming the suitability of the blends for engine application while minimizing risks to efficiency and emission compliance.

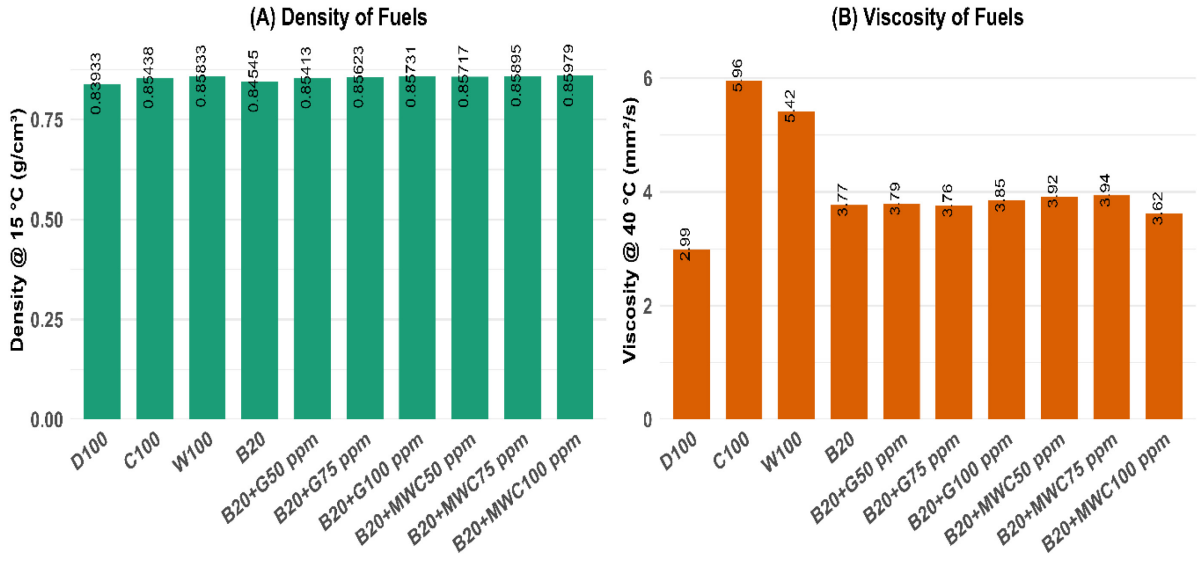

Figure 7. Effect of nanoparticles on fuel: (A) Density, and (B) Viscosity

Calorific value and flash point. The effect of nanoparticles on the calorific value and flash point is illustrated in **Figure 8**. The calorific value, which indicates the energy content of the fuel, shows significant variation among the tested samples as illustrated in **Figure 8A**. Diesel fuel (D100) has the highest calorific value at 42.401 MJ/kg, making it the most energy-dense fuel. On the other hand, the B20 blend (39.403 MJ/kg) has a higher calorific value than pure biodiesels (W100 and C100), which recorded lower values of 36.052 MJ/kg and 35.318 MJ/kg, respectively, due to the presence of the energy-rich diesel fraction. This decrease is mainly caused by the higher oxygen content in biodiesel, which increases the energy used in vaporizing and breaking down oxygenated compounds during combustion, resulting in lower overall heat release [48]. From an engineering perspective, fuels with lower calorific values can lead to higher brake-specific fuel consumption and reduced thermal efficiency, while higher calorific values are advantageous for maintaining engine power output and reducing fuel use.

Incorporating nanoparticles into B20 further increased the calorific value, with B20+GNPs ranging from 39.417 MJ/kg to 40.104 MJ/kg and B20+MWCNTs from 39.571 MJ/kg to 40.517 MJ/kg. This trend can be linked to improved combustion efficiency due to the catalytic activity of nanoparticles, which enhance atomization, oxygen availability, and heat transfer. MWCNTs surpass GNPs in calorific value possibly due to their higher carbon content, better combustion efficiency, and lower oxygen content, all of which help produce more heat in biodiesel blends. The highest calorific value was observed in B20+MWCNT100 ppm (40.517 MJ/kg), indicating that MWCNTs are more effective than graphene in increasing fuel energy density at similar concentrations. A higher calorific value not only improves energy efficiency but also reduces incomplete combustion, thereby lowering emissions of CO and unburned hydrocarbons. A similar pattern was reported by Gad *et al.* [47], who investigated biodiesel produced from waste cooking oil (WCO), with an energy content of 39.4 MJ/kg, and its B20 blend (41.50 MJ/kg) doped with carbon nanotubes (CNTs) and graphene nanosheets (CNSs) at 25 ppm, 50 ppm, and 100 ppm of concentrations. The highest energy values were observed for B20CNT100 and B20CNS100, which recorded 41.480 MJ/kg and 41.497 MJ/kg, respectively.

Figure 8B shows that the flash points of pure biodiesels, C100 and W100, are significantly higher, at 80 °C and 70 °C, respectively, compared to diesel, which has a flash point of 45 °C. This indicates that biodiesels are less volatile, making them safer to store and handle due to their lower ignition risk at reduced temperatures. The B20 blend has a lower flash point of 40 °C, indicating increased volatility compared to pure diesel (45 °C), likely due to the presence of residual methanol in the biodiesel component. Adding graphene nanoparticles results in a non-linear trend: a decrease to 35 °C at 50 ppm, followed by increases to 45 °C and 65 °C at 75 and 100 ppm, suggesting improved thermal stability at higher concentrations. In contrast, MWCNTs provide a more consistent improvement, with flash points rising to 75 °C (50 ppm) and peaking at 90 °C (75 ppm), then slightly dropping to 65 °C (100 ppm). This shows that MWCNTs are more effective at stabilizing the blend, likely due to their dispersion stability and stronger interaction with fuel molecules. From a practical viewpoint, higher flash points enhance operational safety by lowering fire hazards during storage and refueling, while also reflecting reduced volatility that contributes to steadier combustion. Conversely, low flash points may raise risks of premature ignition or vapor formation, which can destabilize combustion and increase pollutant formation.

A similar trend was reported by Gawonou *et al.* [19], who investigated diesel – biodiesel blends with a flash point of 40 °C alongside blends doped with graphene nanoparticles (GNPs) and graphene oxide (GO) at concentrations of 25 ppm, 50 ppm, and 100 ppm. The flash points for the GNP-enhanced blends were observed as 64 °C, 62 °C, and 51 °C, while those for the GO-enhanced blends were 36 °C, 39 °C, and 59 °C, respectively. These findings highlight that nanoparticle additives can strongly influence volatility and safety characteristics, and when carefully optimized, can support both safe handling and efficient, cleaner engine operation.

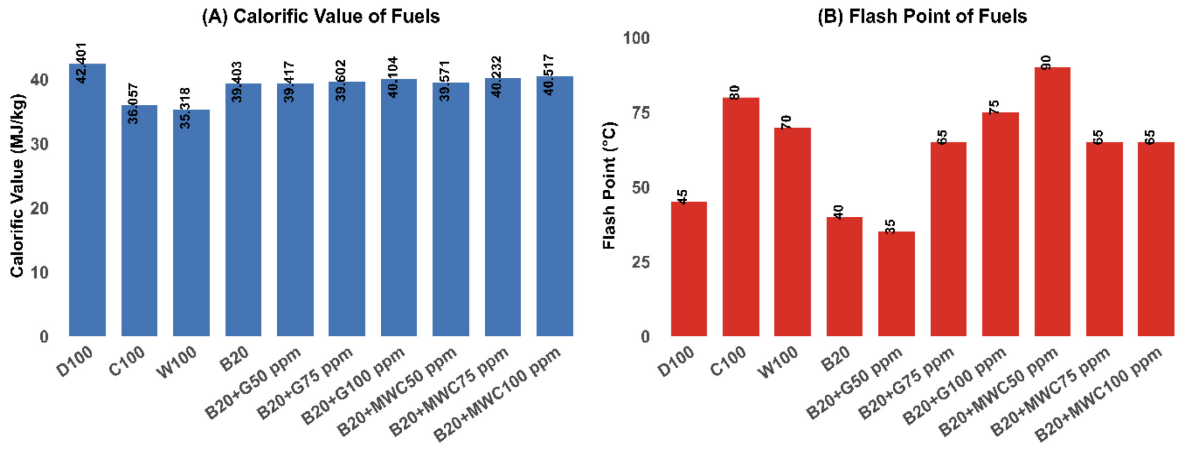

Figure 8. Effect of nanoparticles on fuel Calorific value (A), and Flash point (B)

CONCLUSION

In this study, biodiesel was produced from Croton oil and waste cooking oil (WCO) using optimized transesterification conditions, achieving high conversion efficiencies of 88.13% and 90.96%, respectively. The physicochemical properties of the resulting biodiesels met ASTM D6751 and EN 14214 specifications, confirming their technical feasibility as alternative fuels. Blending with diesel (B20) improved cold flow and combustion characteristics, while doping with carbon-based nanoparticles (graphene nanoplatelets and MWCNTs) further enhanced viscosity, calorific value, Iodine number, water content and CFPP. Among the tested additives, MWCNTs at 75 – 100 ppm consistently delivered the most favorable performance, achieving the highest calorific value (40.52 MJ/kg), and lowest viscosity of 3.62 mm²/s, improved cold flow operability (CFPP – 12 °C), and stable flash point values. These results demonstrate that Croton – WCO biodiesel blends can be considered as viable alternatives to fossil diesel and can have a positive impact and address common biodiesel drawbacks, such as poor atomization, injector fouling, and incomplete combustion, thereby improving reliability in compression ignition engines. Further studies are underway to evaluate engine performance to establish the actual performance of the fuel blends as alternative fuel for the diesel engine.

ACKNOWLEDGMENT

The authors acknowledge the financial support of the African Union (AU) through the Pan African University Institute for Basic Sciences, Technology and Innovation (PAUSTI).

NOMENCLATURE

Abbreviations

B100	100% WCB (80% Waste Cooking and 20% Croton Biodiesel)
B20	20% WCB + 80% diesel
B20+G50 ppm	20% WCB + 80% diesel + 50 ppm of graphene
B20+G75 ppm	20% WCB + 80% diesel + 75 ppm of graphene
B20 + G100 ppm	20% WCB + 80% diesel + 100 ppm of graphene
B20+MWC50 ppm	20% WCB + 80% diesel + 50 ppm of MWCNTs
B20+MWC75 ppm	20% WCB + 80% diesel + 75 ppm of MWCNTs
B20+MWC100 ppm	20% WCB + 80% diesel + 100 ppm of MWCNTs
C100	100% Croton Biodiesel
CFPP	Cold Filter Plugging Point
D100	100% diesel
FAMEs	fatty acid methyl esters

FTIR	Fourier Transform Infrared Spectroscopy
GC-MS	Gas Chromatography-Mass Spectrometry
GNPs	Graphene Nanoparticles
MWCNTs	Multi-Walled Carbon Nanotubes
SEM	Scanning Electron Microscopy
TEM	Transmission Electron Microscopy
W100	100 % Waste cooking oil biodiesel
WCO	Waste Cooking Oil

REFERENCES

1. I. A. Reşitoğlu, K. Altinişik, and A. Keskin, "The pollutant emissions from diesel-engine vehicles and exhaust aftertreatment systems," *Clean Technol. Environ. Policy*, vol. 17, no. 1, pp. 15–27, 2015, https://doi.org/10.1007/s10098-014-0793-9.
2. J. Xue, T. E. Grift, and A. C. Hansen, "Effect of biodiesel on engine performances and emissions," *Renew. Sustain. Energy Rev.*, vol. 15, no. 2, pp. 1098–1116, 2011, https://doi.org/10.1016/j.rser.2010.11.016.
3. D. Neupane, "Biofuels from Renewable Sources, a Potential Option for Biodiesel Production," *Bioengineering*, vol. 10, no. 1, 2023, https://doi.org/10.3390/bioengineering10010029.
4. I. Purnama *et al.*, "Environmental Impacts and the Food vs. Fuel Debate: A Critical Review of Palm Oil as Biodiesel," *GCB Bioenergy*, vol. 17, no. 6, 2025, https://doi.org/10.1111/gcbb.70043.
5. M. Mo, M. G. Rasul, N. M. S. Hassan, H. H. Masjuki, and M. A. Kalam, "Assessment of Physical , Chemical , and Tribological Properties of Different Biodiesel Fuels," 2017, https://doi.org/10.1016/B978-0-12-805423-9.00014-4.
6. K. Chaudhari, N. P. Salunke, and V. R. Diware, "A comprehensive review on performance improvement of diesel and biodiesel fueled ci engines using additives," *Int. J. Performability Eng.*, vol. 17, no. 9, pp. 815–824, 2021, https://doi.org/10.23940/ijpe.21.09.p8.815824.
7. P. M. Ejikeme *et al.*, "Catalysis in biodiesel production by transesterification processes-an insight," *E-Journal Chem.*, vol. 7, no. 4, pp. 1120–1132, 2010, https://doi.org/10.1155/2010/689051.
8. Mathew, G. M., Raina, D., Narisetty, V., Kumar, V., Saran, S., Pugazhendi, A., Sindhu, R., Pandey, A., & Binod, P., Ashok Pandey, "Recent advances in biodiesel production: Challenges and solutions," *Sci. Total Environ.*, vol. 794, p. 148751, 2021, https://doi.org/10.1016/j.scitotenv.2021.148751.
9. B. Tesfa, R. Mishra, C. Zhang, F. Gu, and A. D. Ball, "Combustion and performance characteristics of CI (compression ignition) engine running with biodiesel," *Energy*, vol. 51, pp. 101–115, 2013, https://doi.org/10.1016/j.energy.2013.01.010.
10. M. Torres García, D. Sánchez Martínez, F. Aguilera Roldán, F. J. Jiménez-Espadafor Aguilar, and E. Carvajal Trujillo, "Mechanical analysis of Genoa 03 stirling engine," J. Sustain. Dev. Energy, Water Environ. Syst., vol. 6, no. 3, pp. 521–533, 2018, https://doi.org/10.13044/j.sdewes.d6.0205.
11. A. D. A. Sulistyo, M. B. Triyono, Z. Arifin, M. J. Purnomo, T. A. Prasetya, and C. T. Harjanto, "The Testing of Waste Cooking Oil as Waste Recycle to Realising Green Technical Vocational Education and Training," J. Sustain. Dev. Energy, Water Environ. Syst., vol. 13, no. 1, pp. 1–14, 2025, https://doi.org/10.13044/j.sdewes.d12.0533.
12. M. Leichter, L. V. Lerman, V. G. Maciel, and A. Passuello, "Environmental Assessment of Urban Public Transport's Shift from Conventional to Electric Buses: a Case Study," J. Sustain. Dev. Energy, Water Environ. Syst., vol. 10, no. 4, pp. 1–18, 2022, https://doi.org/10.13044/j.sdewes.d10.0418.

13. T. M. Ismail, D. Lu, K. Ramzy, M. Abd El-Salam, G. Yu, and M. A. Elkady, "Experimental and theoretical investigation on the performance of a biodiesel-powered engine from plant seeds in Egypt," *Energy*, vol. 189, p. 116197, 2019, https://doi.org/10.1016/j.energy.2019.116197.
14. S. S. Hoseini, G. Najafi, B. Ghobadian, R. Mamat, M. T. Ebadi, and T. Yusaf, "Novel environmentally friendly fuel: The effects of nanographene oxide additives on the performance and emission characteristics of diesel engines fuelled with Ailanthus altissima biodiesel," *Renew. Energy*, vol. 125, pp. 283–294, 2018, https://doi.org/10.1016/j.renene.2018.02.104.
15. S. S. Hoseini, G. Najafi, B. Ghobadian, M. T. Ebadi, R. Mamat, and T. Yusaf, "Biodiesels from three feedstock: The effect of graphene oxide (GO) nanoparticles diesel engine parameters fuelled with biodiesel," *Renew. Energy*, vol. 145, pp. 190–201, 2020, https://doi.org/10.1016/j.renene.2019.06.020.
16. A. N. Phan and T. M. Phan, "Biodiesel production from waste cooking oils," *Fuel*, vol. 87, no. 17–18, pp. 3490–3496, https://doi.org/10.1016/j.fuel.2008.07.008.
17. G. Kafuku and M. Mbarawa, "Biodiesel production from Croton megalocarpus oil and its process optimization," *Fuel*, vol. 89, no. 9, pp. 2556–2560, 2010, https://doi.org/10.1016/j.fuel.2010.03.039.
18. G. Kafuku, M. K. Lam, J. Kansedo, K. T. Lee, and M. Mbarawa, "Croton megalocarpus oil: A feasible non-edible oil source for biodiesel production," *Bioresour. Technol.*, vol. 101, no. 18, pp. 7000–7004, 2010, https://doi.org/10.1016/j.biortech.2010.03.144.
19. K. Gawonou, A. Djagni, H. Ndiritu, M. Hawi, and R. Kiplimo, "Biodiesel Production and Characterization for Croton Oil Methyl Ester and Its Blends with Graphene and Graphene Oxide Nanoparticles," vol. 69, no. 12, pp. 120–126, 2021, https://doi.org/10.14445/22315381/IJETT-V69I12P214.
20. K. Kumar and M. P. Sharma, "Performance and emission characteristics of a diesel engine fuelled with biodiesel blends," *Int. J. Renew. Energy Res.*, vol. 6, no. 2, pp. 658–662, 2016, https://doi.org/10.20508/ijrer.v6i2.3827.g6831.
21. T. Wambui, M. Hawi, F. Njoka, and J. Kamau, "Performance enhancement and emissions reduction in a diesel engine using oleander and croton biodiesel doped with graphene nanoparticles," *Int. J. Renew. Energy Dev.*, vol. 12, no. 3, pp. 635–647, 2023, https://doi.org/10.14710/ijred.2023.51785.
22. S. S. Hoseini, G. Najafi, B. Ghobadian, M. T. Ebadi, R. Mamat, and T. Yusaf, "Performance and emission characteristics of a CI engine using graphene oxide (GO) nano-particles additives in biodiesel-diesel blends," *Renew. Energy*, vol. 145, pp. 458–465, 2020, https://doi.org/10.1016/j.renene.2019.06.006.
23. A. I. EL-Seesy and H. Hassan, *Investigation of the effect of adding graphene oxide, graphene nanoplatelet, and multiwalled carbon nanotube additives with n-butanol-Jatropha methyl ester on a diesel engine performance*, vol. 132. Elsevier B.V., 2019. https://doi.org/10.1016/j.renene.2018.08.026.
24. N. Nisar et *al.*, "Brassicaceae family oil methyl esters blended with ultra-low sulphur diesel fuel (ULSD): Comparison of fuel properties with fuel standards," *Renew. Energy*, vol. 117, pp. 393–403, Mar. 2018, https://doi.org/10.1016/J.RENENE.2017.10.087.
25. W. O. Osawa, J. M. Onyari, P. K. Sahoo, and F. J. Mulaa, "Process optimization for production of biodiesel from croton oil using two-stage process," *IOSR J. Environ. Sci. Toxicol. Food Technol.*, vol. 8, no. 11, pp. 49–54, 2014, https://doi.org/10.9790/2402-081134954.
26. S. Debbarma, R. D. Misra, and B. Das, "Performance of graphene-added palm biodiesel in a diesel engine," *Clean Technol. Environ. Policy*, vol. 22, no. 2, pp. 523–534, 2020, https://doi.org/10.1007/s10098-019-01800-2.

27. A. Sivalingam, E. Perumal Venkatesan, K. L. Roberts, and M. Asif, "Potential Effect of Lemon Peel Oil with Novel Eco-Friendly and Biodegradable Emulsion in Un-Modified Diesel Engine," *ACS Omega*, vol. 8, no. 21, pp. 18566–18581, 2023, https://doi.org/10.1021/acsomega.3c00325.
28. R. Atif, I. Shyha, and F. Inam, "Mechanical, thermal, and electrical properties of graphene-epoxy nanocomposites-A review," *Polymers (Basel).*, vol. 8, no. 8, 2016, https://doi.org/10.3390/polym8080281.
29. R. Purohit, K. Purohit, S. Rana, R. S. Rana, and V. Patel, "Carbon Nanotubes and Their Growth Methods," *Procedia Mater. Sci.*, vol. 6, no. Icmpc, pp. 716–728, 2014, https://doi.org/10.1016/j.mspro.2014.07.088.
30. H. Elimam, A. M. Sayed, and A. El Raey, "Alzheimer potential and the metabolic pro fi ling of Sabal blackburniana grown in Egypt supported by molecular modelling †," pp. 18009–18025, 2021, https://doi.org/10.1039/d1ra01725j.
31. M. Elkelawy, E. S. A. El Shenawy, H. A. E. Bastawissi, and M. M. Shams, "Impact of Carbon Nanotubes and Graphene Oxide Nanomaterials on the Performance and Emissions of Diesel Engine Fueled with Diesel/Biodiesel Blend," *Processes*, vol. 11, no. 11, 2023, https://doi.org/10.3390/pr11113204.
32. W. B. Zhang, "Review on analysis of biodiesel with infrared spectroscopy," *Renew. Sustain. Energy Rev.*, vol. 16, no. 8, pp. 6048–6058, 2012, https://doi.org/10.1016/j.rser.2012.07.003.
33. M. F. F. Kamaronzaman, H. Kahar, N. Hassan, M. F. Hanafi, and N. Sapawe, "Analysis of biodiesel product derived from waste cooking oil using fourier transform infrared spectroscopy," *Mater. Today Proc.*, vol. 31, pp. 329–332, 2020, https://doi.org/10.1016/j.matpr.2020.06.088.
34. J. Goli and O. Sahu, "Development of heterogeneous alkali catalyst from waste chicken eggshell for biodiesel production," *Renew. Energy*, vol. 128, pp. 142–154, 2018, https://doi.org/10.1016/j.renene.2018.05.048.
35. A. Matwijczuk *et al.*, "Spectroscopic studies of the quality of WCO (Waste Cooking Oil) fatty acid methyl esters," *BIO Web Conf.*, vol. 10, p. 02019, 2018, https://doi.org/10.1051/BIOCONF/20181002019.
36. M. G. Nespeca, R. R. Hatanaka, D. L. Flumignan, and J. E. De Oliveira, "Rapid and Simultaneous Prediction of Eight Diesel Quality Parameters through ATR-FTIR Analysis," *J. Anal. Methods Chem.*, vol. 2018, 2018, https://doi.org/10.1155/2018/1795624.
37. M. Rosset and O. W. Perez-Lopez, "FTIR spectroscopy analysis for monitoring biodiesel production by heterogeneous catalyst," *Vib. Spectrosc.*, vol. 105, p. 102990, Nov. 2019, https://doi.org/10.1016/J.VIBSPEC.2019.102990.
38. A. B. D. Nandiyanto, R. Oktiani, and R. Ragadhita, "How to read and interpret ftir spectroscope of organic material," *Indones. J. Sci. Technol.*, vol. 4, no. 1, pp. 97–118, 2019, https://doi.org/10.17509/ijost.v4i1.15806.
39. A. Eladeb, "Magnesium Oxide (MgO) as a Sustainable Catalyst for Biodiesel Production from Waste Cooking Oil: A Comparative Study with KOH," *Eng. Technol. Appl. Sci. Res.*, vol. 14, no. 2, pp. 13751–13756, 2024, https://doi.org/10.48084/etasr.7055.
40. A. I. El-seesy, H. Hassan, and S. Ookawara, "Effects of graphene nanoplatelet addition to jatropha Biodiesel e Diesel mixture on the performance and emission characteristics of a diesel engine," *Energy*, vol. 147, pp. 1129–1152, 2018, https://doi.org/10.1016/j.energy.2018.01.108.
41. S. T. Keera, S. M. El Sabagh, and A. R. Taman, "Castor oil biodiesel production and optimization," *Egypt. J. Pet.*, vol. 27, no. 4, pp. 979–984, Dec. 2018, https://doi.org/10.1016/J.EJPE.2018.02.007.

42. M. G. Bidir, N. K. Millerjothi, M. S. Adaramola, and F. Y. Hagos, "The role of nanoparticles on biofuel production and as an additive in ternary blend fuelled diesel engine: A review," *Energy Reports*, vol. 7, pp. 3614–3627, 2021, https://doi.org/10.1016/j.egyr.2021.05.084.
43. J. Sadhik Basha and R. B. Anand, "Performance, emission and combustion characteristics of a diesel engine using Carbon Nanotubes blended Jatropha Methyl Ester Emulsions," *Alexandria Eng. J.*, vol. 53, no. 2, pp. 259–273, 2014, https://doi.org/10.1016/j.aej.2014.04.001.
44. J. Lv, S. Wang, and B. Meng, "The Effects of Nano-Additives Added to Diesel-Biodiesel Fuel Blends on Combustion and Emission Characteristics of Diesel Engine: A Review," *Energies*, vol. 15, no. 3, 2022, https://doi.org/10.3390/en15031032.
45. J. B. Ooi, C. C. Kau, D. N. Manoharan, X. Wang, M. V. Tran, and Y. M. Hung, "Effects of multi-walled carbon nanotubes on the combustion, performance, and emission characteristics of a single-cylinder diesel engine fueled with palm-oil biodiesel-diesel blend," *Energy*, vol. 281, no. May, p. 128350, 2023, https://doi.org/10.1016/j.energy.2023.128350.
46. A. I. El-Seesy, A. K. Abdel-Rahman, M. Bady, and S. Ookawara, "Performance, combustion, and emission characteristics of a diesel engine fueled by biodiesel-diesel mixtures with multi-walled carbon nanotubes additives," *Energy Convers. Manag.*, vol. 135, pp. 373–393, 2017, https://doi.org/10.1016/j.enconman.2016.12.090.
47. M. S. Gad, B. M. Kamel, and I. Anjum Badruddin, "Improving the diesel engine performance, emissions and combustion characteristics using biodiesel with carbon nanomaterials," *Fuel*, vol. 288, no. July, p. 119665, 2021, https://doi.org/10.1016/j.fuel.2020.119665.
48. A. Demirbas, "Importance of biodiesel as transportation fuel," *Energy Policy*, vol. 35, no. 9, pp. 4661–4670, 2007, https://doi.org/10.1016/j.enpol.2007.04.003.

APPENDIX

Table 1 summarizes the physicochemical properties of Croton oil and waste cooking oil (WCO), including mean values and standard deviations (n = 3). The results show that WCO has a significantly higher viscosity (33.60 ± 1.32 mm²/s) compared to Croton oil (23.19 ± 1.08 mm²/s), a characteristic that can hinder atomization and combustion if not corrected through blending or transesterification. Both oils exhibit comparable densities (0.90 ± 0.01 g/cm³ for Croton and 0.89 ± 0.01 g/cm³ for WCO), which fall within the range of typical biodiesel feedstocks. In terms of energy content, Croton oil recorded a slightly higher calorific value (33.09 ± 0.15 MJ/kg) than WCO (32.21 ± 0.14 MJ/kg), although both are lower than petroleum diesel. The acid value and free fatty acid (FFA) content of Croton oil (4.48 ± 0.05 mg KOH/g; 8.57 ± 0.12%) were considerably higher than those of WCO (3.57 ± 0.04 mg KOH/g; 1.10 ± 0.03%), indicating that Croton oil is more prone to oxidation and polymerization, thereby requiring careful catalyst optimization or pre-treatment prior to transesterification. Similarly, Croton oil showed a higher iodine number (150.58 ± 1.25 g I_2/100 g) compared to WCO (136.33 ± 1.18 g I_2/100 g), reflecting its greater degree of unsaturation and suggesting potential susceptibility to oxidative instability during storage. Moisture contents in both oils remained low (0.07 ± 0.01% for Croton and 0.24 ± 0.02% for WCO), which is favourable since excess water can promote soap formation during transesterification and reduce biodiesel yields. These results highlight that Croton oil, despite its higher energy content and reactivity, has limitations due to its elevated acidity and unsaturation, while WCO, although more viscous, offers greater stability. Blending the two oils therefore leverages their complementary properties, producing a biodiesel feedstock with improved balance between yield, stability, and energy content.

Table 2 presents the physical characteristics of the MWCNTs and GNPs employed as fuel additives in this study. Both nanoparticles were supplied by NANOSHEL and appear black in

color, typical of carbon nanomaterials. MWCNTs exhibit a cylindrical morphology with diameters ranging between 10–20 nm and lengths of 3–8 μm, resulting in high aspect ratios that provide extensive surface area for interaction with the fuel matrix. Their average interlayer spacing is approximately 0.34 nm, consistent with the graphitic nature of the nanotubes. The special surface area of MWCNTs is relatively high (90–350 m^2/g), enhancing their catalytic potential and dispersion within biodiesel–diesel blends. GNPs display a flaky morphology with a much smaller thickness (2–4 nm) and lateral dimensions of around 5 μm. Although the interlayer spacing and surface area data are not provided by the supplier, their layered structure and high purity (99.50%) suggest favorable characteristics for modifying fuel properties. The bulk density of GNPs is ~0.10 g/ml, close to the lower end of the range for MWCNTs (0.05–0.17 g/cm^3), but their real density is slightly higher (~2.30 g/cm^3 compared to 1–2 g/cm^3 for MWCNTs). The high purity of both nanoparticles (>99%) ensures minimal interference from contaminants, making them suitable for experimental use in combustion applications. The differences in morphology and surface characteristics between MWCNTs and GNPs imply that they may influence biodiesel properties in distinct ways. MWCNTs, with their large aspect ratio and tunable surface area, are expected to act as effective dispersants and potential micro-catalysts during combustion, while GNPs, with their thin layered structure, may enhance stability and modify cold flow behavior by influencing intermolecular interactions within the blends. These expectations are consistent with earlier reports that carbon nanomaterials can improve atomization, combustion efficiency, and cold flow properties when incorporated into biodiesel–diesel blends.

Various proportions of waste cooking oil and Croton oil biodiesels were blended to determine the optimal ratio for achieving the most favourable properties, as illustrated in the **Table 7**. The results revealed that a blend consisting of 80% WCO biodiesel and 20% Croton biodiesel showed the lowest viscosity, while density and calorific value indicated the best performance, and this blend was named WCB. The WCB is the optimal composition due to its lowest viscosity, suitable density, and highest calorific value among all blends, considering that Croton biodiesel has higher viscosity than WCO biodiesel, while WCO is commercially cheaper and more readily available.

Table 7. Physicochemical properties of croton-waste cooking biodiesel blend at different ratios

		Fuel Properties		
Croton (%)	WC (%)	Density @15 °C (g/cm3)	Viscosity @ 40 °C (mm2 /s)	Calorific value MJ/kg
0	100	0.8544	5.42	36.052
20	80	0.8547	5.47	36.150
30	70	0.8542	5.79	35.942
40	60	0.8591	5.84	35.931
60	40	0.8497	5.97	35.901
70	30	0.8501	5.98	35.731
80	20	0.8507	5.93	35.701
100	0	0.8583	5.96	35.318

Paper submitted: 09.07.2025
Paper revised: 01.11.2025
Paper accepted: 04.11.2025